Mechanistic Insights into Copper(I) and Copper (II) Cation Exchange Reactions in CdSe Nanoplatelets

Progna Banerjee[1], Alexander S. Filatov[2], Xiaobing Zuo[4], Benjamin T. Diroll[1], & Elena V. Shevchenko[1,2,3]**

[1]Center for Nanoscale Materials, Argonne National Laboratory, Argonne, Illinois 60439, USA

[2]Department of Chemistry and [3]James Franck Institute, University of Chicago, Chicago, Illinois 60637, USA

[4]X-ray Science Division, Advanced Photon Source, Argonne National Laboratory, Lemont, IL 60439, USA

** Corresponding authors*

*Emails: prognaphysics@gmail.com eshevchenko@anl.gov

KEYWORDS. 2D Nanoplatelets, Cation Exchange Reaction, Hard Acid-Soft Base, Cadmium Selenide, Copper Selenide

ABSTRACT

In this study, we investigated the synthesis of copper selenide nanoplatelets (NPLs) through a cation exchange reaction (CER) in 5 monolayers thick CdSe NPLs using Cu(I) and Cu(II) precursors. We discovered that the exposure of CdSe NPLs to Cu(I) precursor led to the transformation of NPLs into $Cu_{2-x}Se$ while maintaining their nanoplatelet morphology. The replacement of Cd(II) with Cu(I) prevailed over the formation of doped structures. In the case of Cu(II) precursor, we observed that Cu(II) was first reduced to Cu(I) before being intercalated into the host lattice, resulting in synthesis of $Cu_{2-x}Se$, similar to CER with Cu(I) precursors but without preservation of the initial morphology of NPLs. Interestingly, the presence of oxygen was found to facilitate the cation exchange processes in CdSe NPLs, whereas a nitrogen atmosphere suppressed the CER. Despite the similar ionic sizes of Cu(I) and Cu(II), the substitution of Cd(II) with Cu(II) was found to be challenging, possibly due to the involvement of redox processes resulting in the significant deterioration of initial CdSe NPLs. We demonstrate that CER can achieve near-complete substitution of cadmium atoms with monovalent copper under room temperature. Understanding the processes involved in CERs is crucial for engineering more complex structures, such as high entropy nanoparticles involving cation exchange with different oxidation states and development of material synthesis using machine learning and artificial intelligence approaches.

INTRODUCTION

Cation exchange (CE)[1-4] is recognized as a promising synthesis strategy to tune the chemical composition of nanoparticles (NPs) which enables design of new complex structures including those with metastable phases [3, 5]. Cation exchange reaction (CER) allows the synthesis of doped and alloyed nanocrystals. Doping of copper[6], gold[7] and silver[8] ions in the host matrix of semiconducting NPs results in energy dependent modulation of their localized surface plasmon resonances (LSPRs). In turn, manganese doping is utilized in perovskites[9] to achieve mid-gap emission[10]. The host cations can be completely replaced with the incoming cations[11]. In this case, anionic framework of the host lattice remains often preserved[5]. However, the CER can also result in the reorganization of the anion framework.[12] The extent of the CER as well as the resulting structures depend on the chemical nature of the guest cation[2], their ionic radii and oxidation states[12], temperature conditions[13], and the choice of ligands and solvation environments[14, 15] used for both host and guest cations. The direction, initiation and extent of CER in a material were proposed to be rationalized through a set of thermodynamic principles called the qualitative Pearson's hard and soft acid and base theory (HSAB), together with solubility product constants (Ksp)[2, 14].

The majority of CER studies on semiconductor NPs were performed with transition metal cations with oxidation state (+1)[2]. Exposure of NPs in solution to the Cu(I) and Ag (I), cations that are known to quickly diffuse into the host lattice and replace cations, allows complete replacement of the initial cations as well as doping of the host lattice[1, 16]. The ionic radii[17] of Cu(I) and Ag(I) are 77 pm and 115 pm, respectively. In the case of CdSe NPs, in which radius of Cd(II) is ~109 pm, these values are smaller and larger than the ionic radius of Cd(II), indicating that, perhaps, the size of the cation does not play a critical role in CERs.

Metal cations with other oxidation states have been also investigated in CERs[18, 19]. In some cases, CERs with cations in oxidation state (II) did not affect the morphology of the host nanoparticles[5, 18]. Thus, Zn(II) cations replace Cd(II) cations in the lattice of CdSe without altering of the morphology of CdSe NPs[18, 20]. However, in some cases, a significant deformation of the host NPs was observed[21]. For instance, exposure of CdSe nanoparticles to Hg(II) was accompanied by their partial deterioration[21]. It was also shown that in $Cu_{2-x}Se$ NPs, Cd(II) can be replaced with either Sn(II) or Sn(IV); however, the valency of tin cations was reported to affect the intermediate steps of the exchange process as well as the structure and composition of the final NPs[22]. Thus, Sn(II) with ionic radius of ~118 pm was able to fully replace smaller Cu (I) ions resulting in the distortion of the anion framework of the initial $Cu_{2-x}Se$ host lattice and formation of orthorhombic phase of SnSe[22] without the formation of Cd-Sn-Se alloys during intermediate steps. In turn, exposure of $Cu_{2-x}Se$ NPs to smaller ~81 pm Sn(IV) cations led to only partial replacement of Cd(II) cations and formation of alloyed $Cu_{2-4y}Sn_ySe$ with preserved anion framework of the host lattice[22]. Moreover, the redox reactions between the introduced cations (Sn(II)) and the cation of the host lattice (Cu(I)) were proposed to play a role affecting the cation exchange processes; however, CER with either Sn(II) or Sn(IV) resulted in the formation of NPs where oxidation state of host atoms was identical to their oxidation state in the introduced precursors[22].

Cation exchange process in II-VI semiconductor host lattice enables the synthesis of copper chalcogenide based NPs[6] that are of interest due to their semiconducting surface plasmonic[23] properties in the NIR region. Selective doping with transition metal cations such as copper and manganese in host lattice is utilized for introducing dopant ion related emission, in addition to excitonic property tuning of the host lattice through defect formation[10]. This optical property modulation of LSPR energy position and bandwidth simultaneously resulting in the enhanced light-matter interactions and tunable optical properties offer a variety of potential applications; including in optoelectronics[24], photocatalysis[25], and sensing energy storage[26] and thermoelectrics[27]. In addition, such nanomaterials have remarkable ionic properties tunable through vacancies[28, 29], composition[30], etc. Copper selenide has many phases and structural forms ranging from stoichiometric[31] α-Cu_2Se, Cu_3Se_2, CuSe, and $CuSe_2$, to non-stoichiometric, $Cu_{2-x}Se$[6, 32, 33]. Cu_2Se is considered to be promising thermoelectric material[27] with a peak zT > 2 due to its very low $\kappa < 1$ $Wm^{-1}K^{-1}$. Moreover, the cationic vacancy-containing $Cu_{2-x}Se$[29] with fcc β-phase revealed superionic conducting properties[6], better electrochemical cycling stability[34] and a larger window of 1-2.5 V against Li over its CuSe and $CuSe_2$ counterparts.

The copper selenides with Cu(II) are also revealing a number of interesting properties. For instance, CuSe thin films were found to be p-type semitransparent highly conducting semiconductors[35] that enabled their applications in thin film solar cells, photodetectors, superionic materials and optical filters, while $CuSe_2$ was reported to superconductor at low temperatures with a transition temperature $T_C \sim 2.4$ K[36]. $CuSe_2$ also revealed a weak ferromagnetic behavior below 31 K implying the possible coexistence of ferromagnetism and superconductivity in this compound[37].

To date, the CER studies focus on utilization of Cu(I) precursors (e.g., tetrakis(acetonitrile) copper hexafluorophosphate[6, 38] and CuI[39]) that enable the synthesis of $Cu_{2-x}Se$ or doped CdSe NPs in which Cu has oxidation (I). Different aspects of cation exchange in wurtzite and zinc blende CdSe clusters[33], quantum dots and quantum rods[1] were extensively studied for doping and full cation replacement. Previously, it was reported that CdSe NPLs have substantially different surface chemistry as compared to CdSe quantum dots such as more labile ligands are located in the vicinity of facet and affect the surface termination[40]. All these factors can have a substantial effect on the mechanism of the CERs in CdSe NPLs and the morphology, composition, and structure of the final product. In the case of NPLs CERs are limited mainly to their use for doping purpose meaning that only small concentration of the guest cations (e.g., copper or mercury) ends up in the host lattice[41-43]. Moreover, CER were not previously reported for synthesis of copper selenides with Cu(II) oxidation state.

Here we explored the synthesis of copper selenide nanoplatelets (NPLs) using Cu(I) and Cu(II) precursors via CER in CdSe NPLs- and unveiled the processes involved in CER with variation in copper valences, oxygen availabilities, and counterion species. We used 5 monolayers (ML) thick NPLs since this morphology enables better visualization of structural, morphological, and compositional changes. Exposure of CdSe NPLs to Cu(I) precursor transform NPLs to $Cu_{2-x}Se$ preserving NPL morphology. However, in the case of Cu(II) precursors, we show that prior to intercalation into the host lattice, Cu(II) is getting reduced to Cu(I) and this process is accompanied by a substantial deterioration of the morphology of NPLs. Surprisingly, the presence of oxygen was found to promote the reduction of Cu(II) and facilitate the cation exchange processes in CdSe NPLs. Under nitrogen atmosphere, the CER is suppressed. We demonstrate that redox processes are playing a substantial role in CER in CdSe NPLs with Cu(II) and even with Cu(II) precursors, the material formed as a result of cation exchange processes is likely to be $Cu_{2-x}Se$ characteristic to CER with Cu(I) precursors.

RESULTS AND DISCUSSIONS

In our study we focused on understanding how the valency of copper precursor affects the cation exchange process and if it possible to synthetize copper selenides NPLs with structures characteristic of copper with oxidation state of (I) and (II). We used tetrakis (acetonitrile) hexafluorophosphate and $Cu(NO_3)_2$ as Cu(I) and Cu(II) precursors, respectively, since these precursors have higher solubility in acetonitrile/methanol solutions used for introduction of the precursors to toluene solutions of CdSe NPLs and they are common copper precursors used in previous studies. Since these common precursors of Cu(I) and Cu(II) precursors do no have the same counter anions, we conducted control experiments that took into account the effect of precursor anions that will be discussed in detail in the sections below. We have also conducted the control experiments with Cu(I) and Cu(II) with the same counter ions such as CuCl and $CuCl_2$ that revealed solubility in mixtures of acetonitrile and alcohols at concentrations comparable to concentrations used in experiments with tetrakis (acetonitrile) hexafluorophosphate and $Cu(NO_3)_2$.

In all experiments we used 5 ML CdSe NPLs (**Figure 1a**) that were synthetized according to the procedure reported in literature[44]. We used 5ML thick NPLs as a model system since such NPLs are substantially less prone to lattice distortions due to bending, twisting, *etc.* as compared to 3 ML and 4 MLs NPLs[45] allowing to minimize the effects of lattice distortions on CER.

As evidenced from TEM data (**Figure 1a)** obtained along the (001) basal crystallographic facets[46], individual NPLs are rectangular in shape with median measurements of ~22 nm and 8 nm along the long and short sides, respectively. Powder XRD pattern obtained for freshly synthetized 5 ML CdSe NPLs (purple pattern in **Figure 1d**) indicates that they have mainly cubic zinc blende (ZB) symmetry.

A. CER with Cu(I) precursor in 5 ML CdSe NPLs under anaerobic conditions:

In the case of CER with II-VI quantum dots, nanocrystals, nanorods and nanowires- most of the studies are conducted using the Cu(I) precursor. Since Cu(I) precursors such as tetrakis (copper) acetonitrile hexafluorophosphate is acutely air sensitive, all the experiments were conducted inside a N_2-filled glovebox. We added different concentrations of Cu(I) precursor dissolved in methanol/acetonitrile solution to toluene solution of 5 ML CdSe NPLs and monitored the compositional and structural transformation using DFTEM, STEM-EDS, XRD and XPS techniques. HR-DFTEM (High-Resolution Dark-Field Transmission Electron Microscopy) data indicate that NPL size distributions in the ensemble remains unchanged throughout the reaction as presented in **Figures 1b, 1c** at 154 nM and 330 nM of added Cu(I), respectively. The ensemble size distribution obtained from TEM images is shown in **Figure S1**. The optical extinction coefficient for these 5 ML NPLs with lateral size measured from DFTEM studies was estimated as $\varepsilon = 7.67 \times 10^{7}\ cm^{-1}M^{-1}$ using NPL specific calculations reported in literature[47]. The optical absorbance changes observed during the colloidal reaction over ~3 h from the onset of CER are depicted in **Figure 1e.** The kinetics of the reaction is observed to be relatively slow compared with CdSe NPs[38] and nanoclusters[33] and complete transformation of CdSe NPLs occurred in ~3h at higher concentration of Cu(I) precursor (~330 nM) with preservation of the NPL morphology throughout.

Previously, the Cu(I) CERs in CdSe quantum dots were reported to occur via cooperative mechanism that was established first via optical spectroscopy[48] and later confirmed by in situ X-ray absorption studies[49]. According to this mechanism, the initial stages of the CER proceed through light doping of the Cu(I) in the CdSe lattice, making it prone to abrupt transition of the quantum dot into copper selenide phase upon reaching a certain point in the CER. We monitored the evolution of the composition of 5ML CdSe NPLs exposed to different concentrations of Cu(I) precursors by performing the EDS analysis (**Figure 1f, Figure S2**). We observed that upon increasing the Cu(I) concentration beyond the critical point, the significant increase of copper concentration in the host CdSe NPLs (**Figure 1f**). However, our copper concentration "jump" was not as abrupt as it was previously reported for CdSe NCs[49, 50]. Therefore, our data are supportive of cooperative mechanism, however, we cannot fully exclude possibility of alloying at later stages of CER previously reported for cation exchange in $Cu_{2-x}Se$ with Sn(IV) cations[22].

We observed that the XRD peaks of the cation exchange product represented with the pink pattern in **Figure 1d** matches with peak position of previously reported $Cu_{1.8}Se$ ($Cu_{1.8}Se$-JCPDF 06-0680). The HAADF and EDS mapping results indicate that cation exchange takes place uniformly in all CdSe NPLs (**Figures 1g-1j**) until full conversion is obtained. The absence of cadmium in the EDS maps (**Figure 1g-1i**) confirmed the full conversion into $Cu_{2-x}Se$ at the single particle level. The advanced stages of the CER with Cu(I) are quantitatively demonstrated in **Figure S3** with HREDS maps.

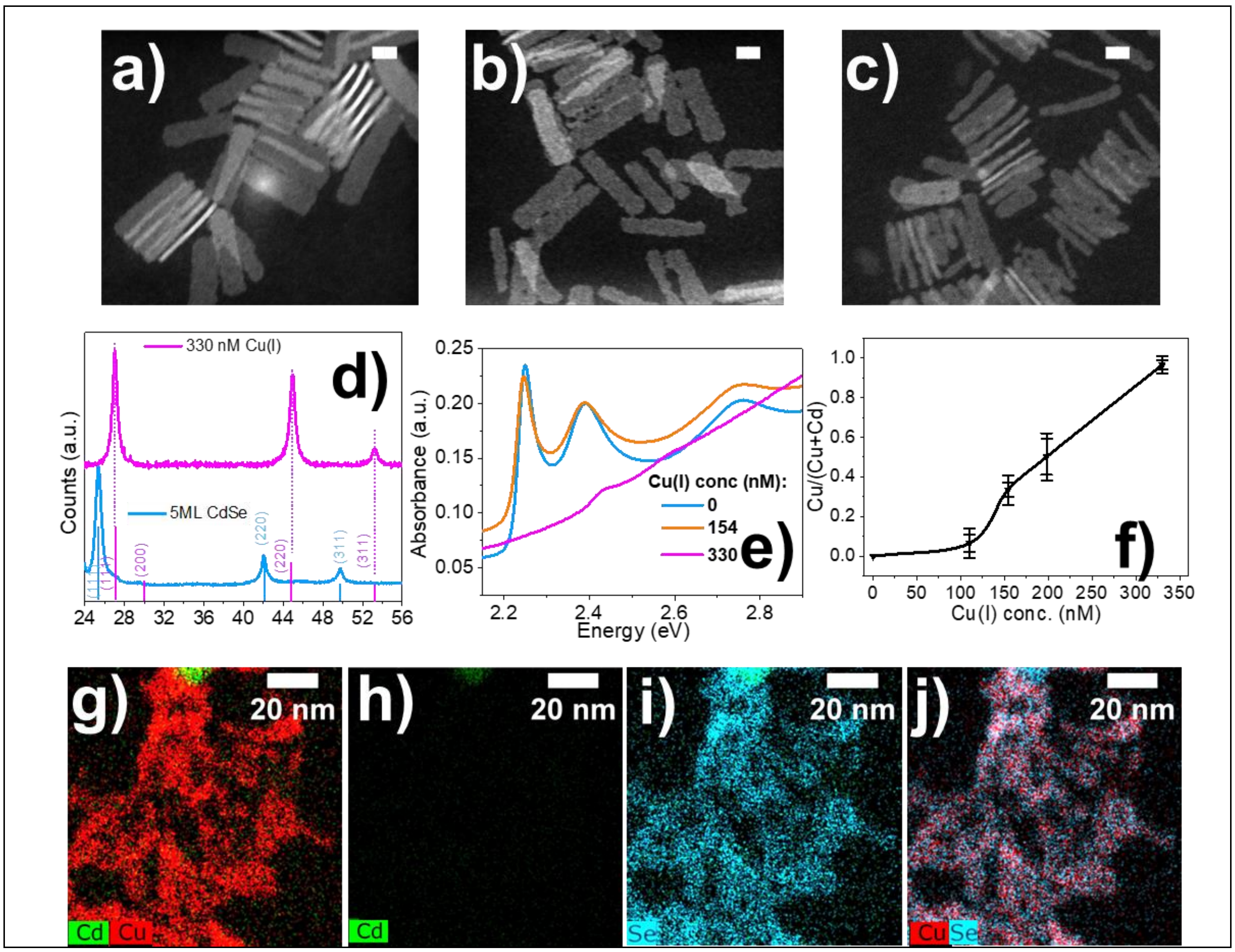

Figure 1. (a-c) The DFTEM images with scalebars of 5 nm each of (a) as-synthetized 5 ML CdSe NPLs and NPLs after their exposure to 154 nM and 330 nM methanol/acetonitrile solution of Cu(I) precursor tetrakis(acetonitrile) copper(I) hexafluorophosphate for 3h (b and c, respectively) demonstrating the preservation of NPLs morphology during cation exchange processes. The XRD patterns with the (hkl) indices indicated (d) of as synthetized 5 ML CdSe NPLs (shown in blue) and final $Cu_{2-x}Se$ NPLs (shown in pink) formed as a result of addition of 330 nM solution of methanol/acetonitrile solution of Cu(I). Solid lines shown in pink and blue correspond to cubic $Cu_{1.8}Se$-JCPDF 06-0680 and cubic ZB CdSe, respectively. (e) The optical absorbance spectra of 5 ML CdSe NPLs acquired after their exposure to different concentrations of Cu(I) precursor for 3 h. (f) Dependance of the concentration (along with error bars) of copper(I) in CdSe NPLs after their exposure to Cu(I) for 3 h determined by EDS analysis on concentration of the Cu(I) precursor. (g-j) EDS maps measured on 5 ML CdSe NPLs exposed to 330 nM solution of Cu(I) precursors for 3h depicting distribution of Cu and Cd (g), Cd (h), Se(I) and superposition of Cu and Se (j).

B. CER of 5 ML CdSe NPLs with Cu(II) precursor:

CER reactions were performed next with a methanol/acetonitrile mixture of Cu(II) solution in nitrate form under anaerobic condition, to mimic the atmospheric reaction parameters of the Cu(I) case closely. We performed UV/Vis spectra (**Figure 2a**) of CdSe NPLs to progress the various stages of the reaction. While no changes in NPLs' morphology was detected by DFTEM upon their exposure to lower concentrations of Cu(II) (**Figure 2b**), their long-term exposure (~3h) to high concentration of Cu(II) precursor (**Figure 2c**) resulted in some etching of the NPLs that is particular apparent at the edges of NPLs. This can point out some redox processes involving Cu(II) and/or possibly traces of oxygen potentially present in N_2. XRD data (**Figure 2d**) obtained on 5 MLs CdSe NPLs exposed to Cu(II) cations under nitrogen flow indicated insignificant quantities of copper selenides formation was observed even in the experiments of high concentrations (330 nM) of Cu(II). HAADF **(Figure 2e**) and EDS maps (**Figures 2f & 2g**) show the presence of significant quantities of unreacted CdSe in these NPLs even at 330 nM addition of the Cu(II) reactant over a course of 3 h reaction time. The 2θ peak at 31.2 º present in the XRD spectrum shown in **Figure 2d** can correspond to small amount of product formed as a result of cation exchange caused by the exposure of the unpurified reaction mixture to ambient conditions prior to solvent/solvent purification step that is discussed below. Next, we performed the same experiments under ambient conditions to shed light on the possible role of oxygen.

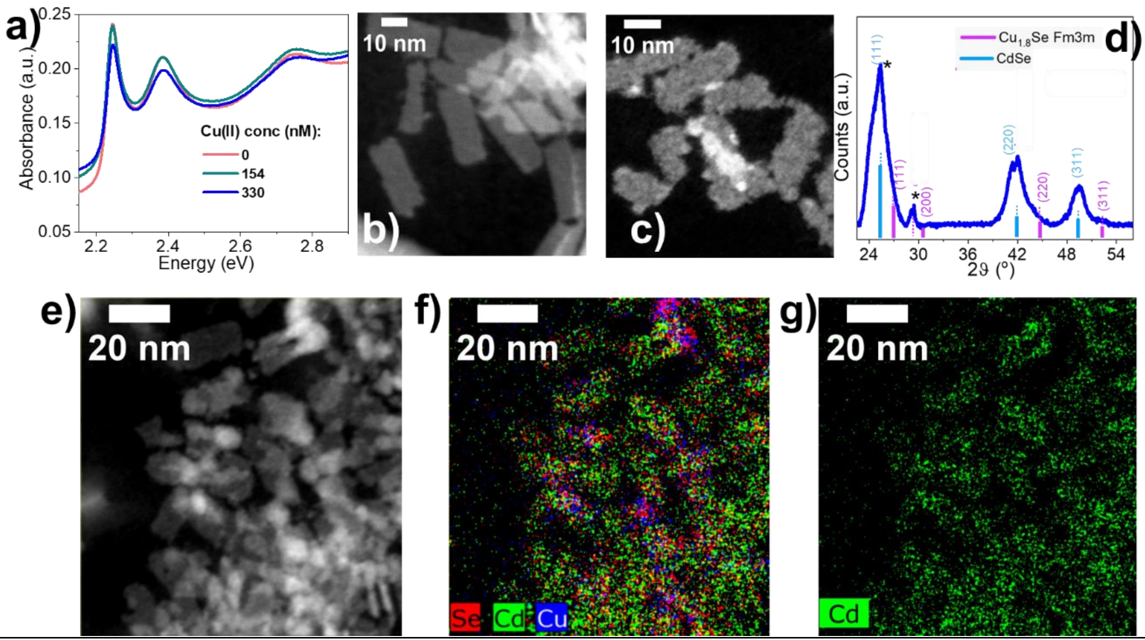

Figure 2. (a) Optical absorbance spectra corresponding to the solutions of 5ML CdSe NPLs after their exposure to different concentrations of methanol/acetonitrile solution of Cu(II) precursor in the form of $Cu(NO_3)_2$ for 3h under N_2 environment. (b, c) DFTEM images of the 5 ML CdSe NPLs after their exposure to 154 nM and 330 nM solutions of methanol/acetonitrile solution $Cu(NO_3)_2$ under N_2 flow for 3 h (b and c, respectively). (d) XRD data on the samples shown in (c) (with the (hkl) indices indicated). (e-g) HAADF image (e) and EDS maps corresponding to Se, Cd and Cu obtained for the sample shown in (c). Solid lines shown in pink and blue correspond to cubic $Cu_{1.8}Se$-JCPDF 06-0680 and cubic ZB CdSe, respectively

Next, we conducted these experiments under ambient conditions (note, both CdSe NPLs in **Figure 3a** and Cu(II) are relatively stable under ambient conditions). Surprisingly, XRD patterns (**Figure 3b**) indicated that the crystalline structure of the formed product is consistent with *fcc* cubic $Cu_{2-x}Se$ suggesting that the Cu(II) was reduced. The shift of peaks at higher 2θs is characteristic to compressive strain caused by small size[51].The smaller concentrations of Cu(II) led to the appearance of low intensity broad peaks those positions match the peak position of Cu_{2-}

$_x$Se. Exposure of CdSe NPLs to various concentrations of Cu(II) results in shift of the positions of the peaks characteristic to ZB structure of CdSe and appearance of rather broad peaks characteristic to cubic $Cu_{2-x}Se$ with accompanying doping-related shifts of the diffraction peaks as typically expected from Vegard's law[38] during CER. A few peaks matching the $Cu(NO_3)_2$ phase provided in **Figure S3** are observed. Considering the substantial etching of the initial 5 ML NPLs upon their exposure to Cu(II) revealed in TEM studies, the broader XRD peaks of the CER product are expected. No indication of the formation of phases characteristic to copper chalcogenides with Cu(II) oxidation state was observed.

We found that the introducing of $Cu(NO_3)_2$ dissolved in methanol/acetonitrile solution mixture to CdSe NPLs in toluene at room temperature was immediately accompanied by substantial changes in optical absorbance spectra (**Figure 3c**), as well as morphological changes revealed by HRTEM studies. The incomplete CE in CdSe NPLs can be attributed to the reduced number of active surface area originating from stacking of NPLs in toluene as it is evidenced from SAXS measurements of NPLs (**Figure 3d)**. The peaks at 0.126, 0.156, 0.2558, 0.314, 0.471 $Å^{-1}$ and higher order q values correspond to the lamellar ordering with 5.4 nm periodicity formed by these NPLs in toluene. More specifically, the intense peak at a scattering vector $q^*=0.126$ $Å^{-1}$ arises from the face-face stacking of the platelets with a period $d=2\pi/q^*=5.4$ nm within the CdSe threads[52]. The NPL thickness is 1.5 nm, the faces of neighboring NPLs are 4.5 nm apart. The additional separation distance of 1.5 nm is reported to be possibly due to partially interdigitated oleic acid molecules bound to the faces of the NPLs[52]. The second intense peak at 0.156 $Å^{-1}$ originates from the NPLs occasionally assembling in face-edge orientation. All NPLs in toluene solution take part in the self-assembly process and none are present as monomers in solution. Hence, this self-assembly[53] of CdSe NPLs in the solution[54] into long-thread-like strands could be a factor which limits the exposure of the NPLs to the copper cations.

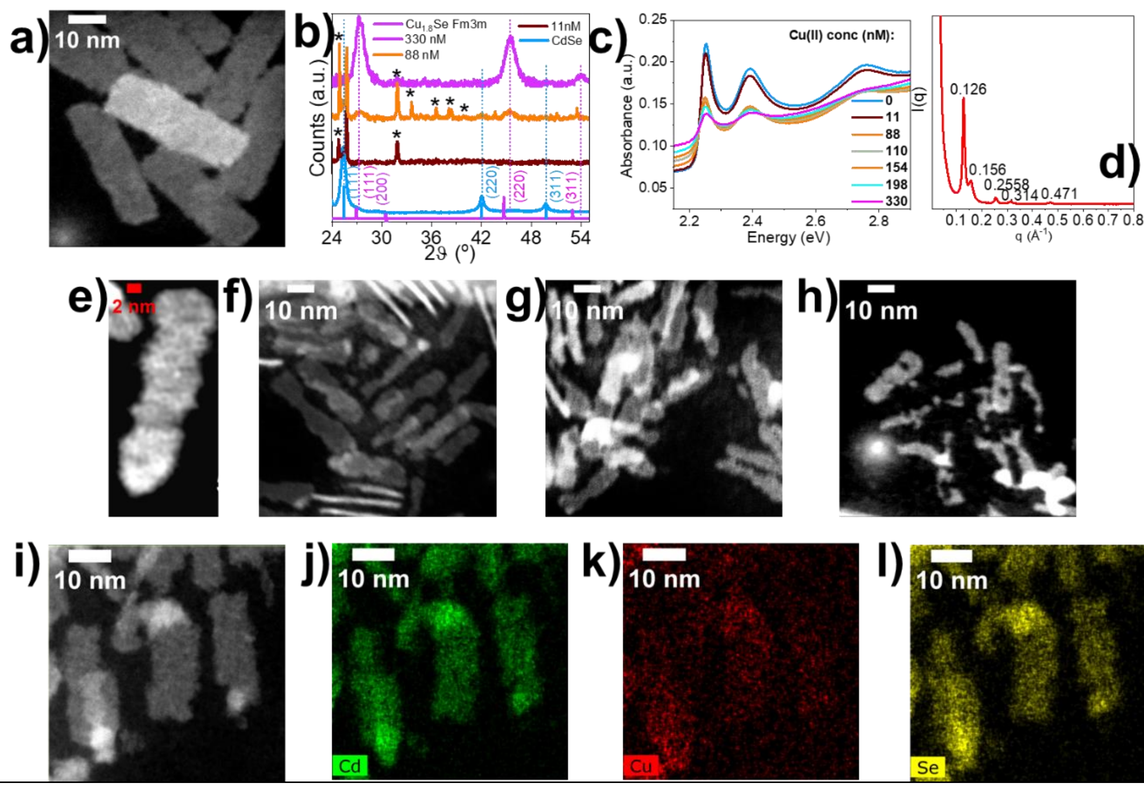

Figure 3. (a) The DFTEM image of as-synthetized 5 ML CdSe NPLs. (b) The XRD patterns with the (hkl) indices indicated when measured for as-synthetized 5 ML CdSe NPLs and after their exposure to different concentrations of methanol/acetonitrile solution of Cu(II) precursor in the form of $Cu(NO_3)_2$ under ambient conditions. Solid lines shown in pink, and blue correspond to cubic $Cu_{1.8}Se$-JCPDF 06-0680 and cubic ZB CdSe, respectively. The stars denote the peaks corresponding to $Cu(NO_3)_2$ used as a precursor. Note, that samples obtained with 11 nM and 88 nM concentrations were not purified before XRD analysis to eliminate the possible effects associated with the purification. (c) Optical absorbance spectra corresponding to the solutions of 5ML CdSe NPLs after their exposure to different concentrations of methanol/acetonitrile solution of Cu(II) for 30 min under ambient environment. (d) SAXS data on CdSe NPLs in toluene revealing the stacking of 5 ML CdSe NPLs in solution. DFTEM data on 5 ML CdSe NPLs exposed for 30 min to different concentrations of methanol/acetonitrile of Cu(II): (e, f) 88 nM, (g) 110 nM and (h) 198 nM. (I) HAADF image and EDS maps for Cd, Cu and Se revealing the elemental distribution in 5 ML CdSe NPLs exposed to 154 nM Cu(II) for 30 min.

We have tested different concentrations of Cu(II) precursor (**Figures 3e**) and observed that even a short time (10 min) exposure of 5 ML CdSe NPLs to even small concentrations of Cu(II) precursor led to etching-related changes in NPLs (**Figure 3e**) that progressively intensifies when higher concentrations of Cu(II) precursor were used (**Figure 3f-h**). HAADF data (**Figure 3i**) revealed the appearance of the segregated brighter areas that potentially can indicate the segregation of elements with high atomic numbers (z) (in this case cadmium). Also, EDS maps for Cd, Cu and Se elements (**Figure 3-i, j, k, l**) indicate that exposure of CdSe NPLs to Cu(II) precursors leads to higher Cd concentration in certain areas of CdSe NPLs (**Figure 3j**) that coincides with areas of higher concentration of Se. The Cd to Se ratio is 0.83 in tip area in **Figure 3j** while as compared to 0.72 characteristic to the entirety of the NPL, with these EDS measurements and relative error estimates tabulated in **Table S1**. These results are indicative of NPLs' etching. Note, that as-synthetized 5 ML CdSe NPLs reveal 1.2 Cd to Se ratio[55]. The lower ratio of Cd to Se in CdSe NPLs exposed to Cu(II) precursor is suggestive of Cd atoms leaving the NPLs.

Since the Cu(I) and Cu(II) precursors have different anions, we next conducted control experiments aimed on elucidation of the role of the precursor anions ions of substituting cation on the probability and kinetics of the cation exchange events in CdSe NPLs. In this set of experiments, we added equivalent nM concentration of ammonium hexafluorophosphate to a methanol/acetonitrile solution of $Cu(NO_3)_2$ and used this mixture in CER with 5ML CdSe NPLs under ambient conditions. In the presence of ammonium hexafluorophosphate, we also observed that Cu(II) causes the substantial morphological changes in CdSe NPLs (**Figure 4a**); however, the monitoring of the absorbance spectra of 5ML CdSe NPs (**Figure 4b**) revealed their substantially slower evolution as compared to the experiments with $Cu(NO_3)_2$ precursor indicating slower kinetics of the cation exchange in the presence of hexafluorophosphate ions. For instance, exitonic features characteristic to 5 ML NPLs are still preserved in the samples after 3 h of their exposure to Cu(II) while in the absence of ammonium hexafluorophosphate all such features were reasonably lost after 1 h. TEM data (**Figure 4a**) indicated the co-existence of totally disintegrated NPLs and those that managed to maintain the nanoplate morphology. The EDS maps (**Figure 4c, d**) show that smaller NPs contain higher concentrations of copper (**Figure 4c**). These data suggest that some NPLs are either more active than others in redox reactions or this can be a result of stacking of CdSe NPLs in the colloidal solution (**Figure 3d**). PL emission time maps with color bars shown in **Figures 4e & f** visualize the delayed reaction kinetics in the presence of the ammonium hexafluorophosphate anion.

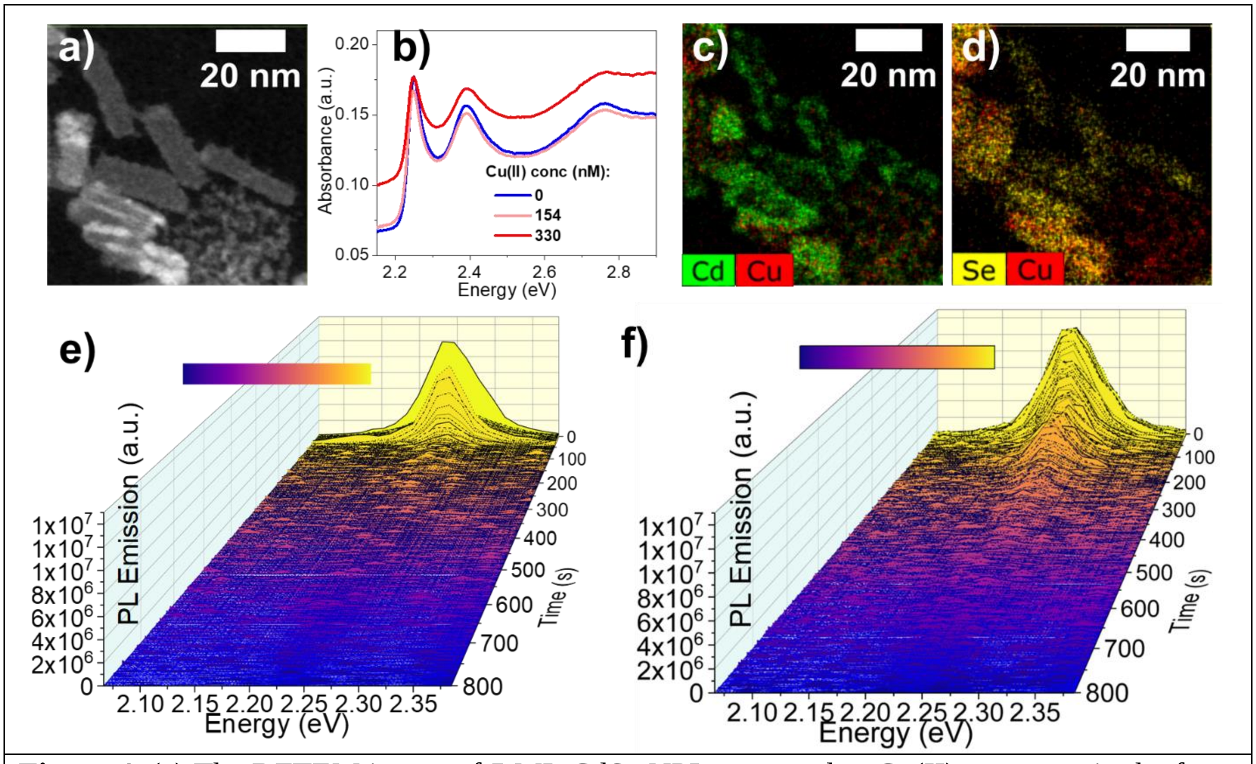

Figure 4. (a) The DFTEM image of 5 ML CdSe NPLs exposed to Cu(II) precursor in the form of $Cu(NO_3)_2$ under ambient conditions for 3 h in presence of ammonium hexafluorophosphate. (b) Optical absorbance spectra corresponding to the solutions of 5ML CdSe NPLs after their exposure to different concentrations of methanol/acetonitrile solution of Cu(II) for 3 h min under ambient environment in presence of ammonium hexafluorophosphate. (c, d) EDS maps for Cd,

Cu and Se revealing the elemental distribution in the sample shown in (a). (e, f) The evolution of the PL emission of the 5 ML CdSe NPLs exposed to Cu(II) under ambient conditions in the absence and in the presence of ammonium hexafluorophosphate anion.

The direction, initiation and continuation of CER in a material system with predetermined host and guest cations are predicted to be determined though the ligation and solvation environment through a set of thermodynamic principles, Pearson's hard and soft acid and base theory (HSAB), together with solubility product constants (K_{sp})[2, 14]. HSAB theory predicts that hard acids prefer to interact with hard bases while soft acids have a greater affinity for soft base[56]. The relative hardness (or softness) of species is determined by its electronic structure, polarizability, and charge density[56, 57] and can be estimated from absolute hardness parameter (η)[58]. CdSe contains hard Lewis acid such as Cd(II) cations with η = 10.29 that can bind more strongly to hard bases, such as NO_3^- that has hardness value of 5.23 or PF_6^- that has hardness of 6.311 than do softer cations such as Cu(I) and Cu(II) with 6.28 and 8.27 hardness's, respectively[59]. In terms of HSAB theory, NO_3^- and PF_6^- anions are strong Lewis bases with η[60, 61] of ~5.23 and 6.311. Therefore, according to HSAB theory we should not expect slower kinetics of cation exchange in the presence of PF_6^- anions shown in **Figure 4**. However, we used NH_4PF_6 as a precursor for PF_6^- anions and, in principle, NH_4^+ cations could form weak complexes with copper precursors or surface cadmium that can limit the available concentration of Cu(II). However, the co-existence of preserved CdSe NPLs with smaller fragments formed as a result of cation exchange reaction with Cu(II) revealed by TEM (**Figure 4a**) as well as preserved exitonic features (**Figures 4b&f**) suggest that, most likely, addition of NH_4PF_6 to the solution of 5 ML CdSe NPLs promoted the assembly of NPLs that, in turn, limited the exposure of the NPLs' surface to the reactive species. Previously, the formation of periodic structures in organic solvents was induced by introducing of ionic species[62].

We did not observe the direct CER with Cu(II). It is worth noting that previously Cu(II) was used as a precursor, however, in presence of a strong reducing agent like trioctylphosphosphine[22, 42], assuming the complete reduction of Cu(II) into Cu(I). However, the presence of unreduced Cu(II) can significantly affect the CER and morphology of NPs. Therefore, understanding of the effect of cation valences on the morphological and compositional transformation is important. In principle, HSAB theory arguments can potentially explain why Cu(II) does not replace cadmium atoms while Cu(I) does since the hardness of Cu(II) is higher than that of Cu(I) (8.27 *vs* 6.28, respectively). Therefore, it is reasonable to expect that Cu(II) atoms can interact efficiently with NO_3^- that has hardness of 5.23 that in turn can limit the availability of Cu(II) precursor for CE.

We also investigated CER using Cu(I) and Cu(II) precursors with the same counter ions such as CuCl and $CuCl_2$ dissolved in methanol/acetonitrile mixture. The results from the CER experiments are displayed in the supplementary file in **Figures S5, S6 and S7**. For the CuCl CER in **Figure S5**, little deterioration is observed in the nanoplatelets with the end product being $Cu_{1.8}Se$. This result agrees with our observations on Cu(I) CER with hexafluorophosphate precursori(**Figure 1)**. For the reaction with Cu(II), shown in **Figure S6**, we observe partial conversion to $Cu_{1.8}Se$, with significant deterioration in the NPL morphology, similar to what was found for $Cu(NO_3)_2$ in **Figure 3**. The CER when performed under N_2 atmosphere, proceeds to completion in the case of Cu(I), while the reaction is arrested for Cu(II) precursor (**Figure S7**). It is worth noting that since Cl^- ion has a very similar base hardness of 5.67 as the NO_3^- that has the hardness of 5.23, similar trends in CER processes are expected for these two copper precursors within HSAB theory.

It is worth noting that we observed that even when we used Cu(II), cation exchange processes in 5 ML CdSe NPLs resulted in the formation of $Cu_{1.8}Se$ NPLs that is similar to the product formed via CER with Cu(I) precursor. However, in the case of Cu(II) precursor, CER is accompanied by a significant deterioration of CdSe NPLs. Analysis of the X-ray photoelectron spectroscopy data demonstrated that copper, cadmium and selenium have similar oxidation state since the peak positions of XPS spectra of samples exposed to the cations either Cu(I) or Cu(II) have similar binding energies (**Figure 5 a, b, c**). The spectrum contains the line-shape information of the deconvoluted peaks and overlaps the raw data in each of the panels shown. However, as compared to initial 5 ML NPLs, the peak positions of selenium and cadmium are shifted toward higher binding energies that can be associated with oxidation. The XPS spectra do not reveal the presence of a representative shake-up peak at ~942-944 eV characteristic to Cu(II) species[63]. Lack of such features and, essentially, the same binding energy shifts suggest similar oxidation states of copper ions in the products obtained via CER with Cu(I) and Cu(II) precursors. These binding energy shifts agree with those previously reported for Cu(I)-containing NPs[63]. The selenium 3d spectra of 5 ML CdSe NPLs as well as of both products (Figure 5) do not reveal $3d_{5/2}$ and $3d_{3/2}$ doublet peaks separated by 0.9 eV spin-orbit coupling with characteristic 3:2 ratio in intensity[63]. This can be indicative of the presence of some oxidized selenium species. The spin-orbit coupling for Se 3d is 0.86 eV and the area ratio of two peaks $3d_{3/2}$ to $3d_{5/2}$ was constrained to 2/3. In face the formation of Se(0) has been previously noticed for selenides kept under ambient conditions[64]. Further, peak shifts, peak broadening and tailing to higher binding energies may suggest existence of small amounts of even more oxidized selenium species[64]. For Cu 2p, the spin-orbit coupling is 19.80 eV and the area ratio of two peaks $2p_{3/2}$ to $2p_{1/2}$ is constrained to 1/2. The spectra were deconvoluted using 2 doublet peaks suggesting a very minor amount of Cu(II). A summary of the XPS results showing the full width at the half maximum and peak positions of the characteristic peaks is provided in the supplementary file Table S2.

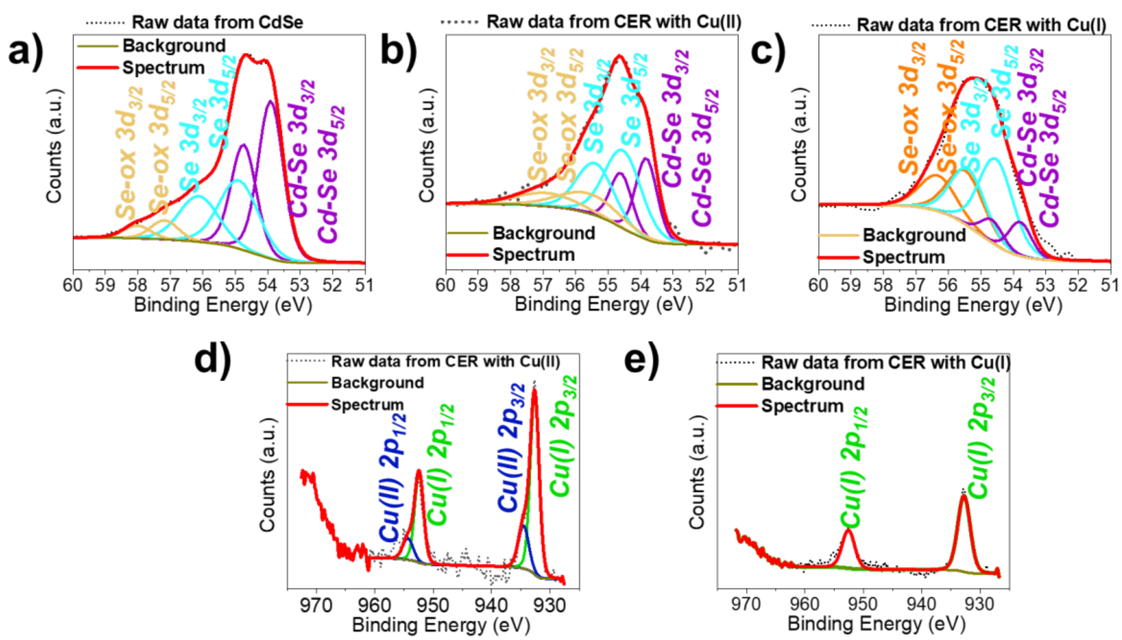

Figure 5. XPS spectra of Se 3d (a-c) and Cu 2p obtained on the as-synthetized 5 ML CdSe NPLs and after their exposure to 154 nM methanol/acetonitrile solutions of Cu(I) and Cu(II) precursors in the form tetrakis(acetonitrile) copper(I) hexafluorophosphate and $Cu(NO_3)_2$, respectively.

CONCLUSIONS

In this study, we investigated the synthesis of copper selenide nanoplatelets (NPLs) using Cu(I) and Cu(II) precursors via cation exchange reaction (CER) in CdSe NPLs. Our aim was to understand the processes involved in cation exchange in CdSe and to observe the changes in structural, morphological, and compositional features using 5 monolayers thick NPLs. We found that exposing CdSe NPLs to Cu(I) precursor transforms the NPLs to $Cu_{2-x}Se$ while preserving their nanoplate morphology. Complete replacement of Cd(II) with Cu(I) dominated over the formation of doped structures. When using Cu(II) precursors, we observed that Cu(II) is reduced to Cu(I) prior to intercalation into the host lattice, which is accompanied by a substantial deterioration of the NPLs' morphology. Interestingly, we discovered that the presence of oxygen promotes the reduction of Cu(II) and facilitates the cation exchange processes in CdSe NPLs. Conversely, under a nitrogen atmosphere, the CER is suppressed. Our results suggest that redox processes play a significant role in CER in CdSe NPLs with Cu(II) precursors, and even with Cu(II) precursors, the material formed as a result of cation exchange processes is likely to be $Cu_{2-x}Se$, which is characteristic of CER with Cu(I) precursors. Despite the similarity of the ionic sizes of Cu(I) and Cu(II), the substitution of Cd(II) with Cu(II) was found to be challenging possibly owing to contribution of the redox processes. Our study advanced the understanding of CER in 5 ML CdSe NPLs with copper precursors with different oxidation states. As compared to earlier studies with copper doping limited to 3.6% or less[42] achieved at elevated temperatures, we demonstrate that CER was able to proceed to near complete substitution of cadmium atoms with monovalent copper at ambient temperature and pressure conditions and under inert atmosphere. Understanding of the processes involved in cation exchange reactions is critical to engineering of more complex structures, such as high entropy nanoparticles which involves the cation exchange processes among cations with different oxidation states[65]. Moreover, careful consideration of all process involved into CER is critical for accelerated development of material synthesis using machine learning and artificial intelligence approaches[66].

METHODS

Chemical reagents. Cadmium nitrate tetrahydrate (99.997%), sodium myristate (≥99%), cadmium(II) acetate (Cd(OAc)2; 99.995%), cadmium acetate dihydrate (Cd(OAc)2.2H2O), selenium powder (Se, ≥99.5%), octadecene (ODE; 90%), oleic acid (OlAc, 90%), copper (II) nitrate hydrate, tetrakis (acetonitrile) copper(I) hexafluorophosphate, ammonium hexafluorophosphate, toluene (98%), anhydrous acetonitrile (99.8%), and methanol were purchased from Sigma Aldrich. All chemicals were used without further purification.

Preparation of Cadmium Myristate. Cadmium nitrate tetrahydrate (1.23 g) was dissolved in 40 mL of methanol and 3.13 g of sodium myristate was dissolved in 250 mL of methanol under strong stirring; these solutions were then combined and stirred approximately one hour. The whitish product was centrifuged, and the white precipitate part was dissolved in methanol. The resulting precipitate of cadmium myristate was filtered and washed several times with methanol for removal of excess precursors and was dried for 24 h under vacuum.

Synthesis of CdSe 5 monolayer (ML) nanoplatelets (NPLs) emitting at 550 nm. The synthesis was performed according to literature[44]. 340 mg of cadmium myristate and 28 mL of ODE are loaded into a 50 mL three-neck flask. The solution is stirred and degassed at room temperature for half an hour and at 95 °C for an hour under vacuum, respectively. After the heating mantle is set to 250 °C, the vacuum is broken at 100 °C and the flask is filled with argon gas. When the temperature of the solution reaches 250 °C, a pre-prepared solution of 24 mg Se dispersed in 2 mL of ODE is swiftly injected into the hot solution. When the color of solution becomes orange, 240 mg of cadmium acetate dehydrate is rapidly introduced. Then, the solution is kept at 250 °C for 10 minutes and 1 mL of OA is injected before cooling down to room temperature using water bath. After size-selective precipitation, the 5 ML NPLs are dissolved and stored in toluene.

Reactions with Cu(II) under aerobic conditions. To a 340 nM concentration solution of NPLs dispersed in toluene, a methanol: acetonitrile solution of Cu(II) precursor in the form of $Cu(NO3)_2$ was added in aliquots of 5 nM under continuous stirring until the final concentration of 330 nm addition was reached within 1 h of start. The reaction was observed using optical absorption and photoluminescence spectroscopy measurements. For the results shown in **anaerobic** case these steps were performed inside the N_2-filled glove box, with the time steps adjusted so the full reaction takes place within 3 h. For reactions with chloride precursors, equivalent molar of copper (II) chloride was dissolved under ambient conditions in a methanol: acetonitrile solution, and equivalent nM aliquots of this precursor was used in CER to 340 nM concentration solution of NPLs dispersed in toluene.

Reactions with Cu(I) under anaerobic conditions. All exchange reactions were carried out in an oxygen-free, moisture-free, N_2-filled glove box. A solution of Cu(I) precursor in the form of tetrakis(acetonitrile) copper(I) hexafluorophosphate ($[(CH3CN)4Cu]PF_6$) in 10% v/v of methanol in acetonitrile was then added dropwise to the 340 nM NPL solution added in aliquots of 5 nM under continuous stirring until the final concentration of 330 nm addition was reached within 3 h of start. Exchange was monitored by ultraviolet-visible absorption spectroscopy photoluminescence spectroscopy. For reactions with chloride precursors, equivalent molar of copper (I) chloride was dissolved under ambient conditions in a methanol: acetonitrile solution, and equivalent nM aliquots of this precursor was used in CER to 340 nM concentration solution of NPLs dispersed in toluene.

Optical absorption and photoluminescence spectroscopy. Ultraviolet-visible absorption spectroscopy measurements were performed using a PerkinElmer Perkin-Elmer Lambda 950. PL emission spectra from solutions were recorded by using Fluorolog iHR 320 Horiba Jobin Yvon spectrofluorometer equipped with a PMT detector.

Transmission electron microscopy imaging and Energy Dispersive Spectroscopy. Elemental analysis was carried out on the CdSe, the intermediate of Cu(II) and Cu(I) reaction products, and the final compositions by STEM/EDS. STEM/EDS was performed on a Talos F200X(S)TEM instrument operating at 200 kV. Samples were prepared by drop-casting NPLs from solution onto ultrathin carbon 300-mesh Au/400-mesh Ni grids from Ted Pella followed by repeated washing of the grid with methanol, acetone and lastly IPA followed by drying under vacuum overnight. A zero-background double-tilt holder was used for STEM/EDS measurements. Data were collected for 40-90 min and the holder was left in the vacuum chamber overnight prior to the experiments to minimize the drift. The atomic %s of Cu, Cd and Se, obtained were converted to atomic ratios by normalizing the Se content to 1. HRTEM and HAADF-STEM images were also acquired this instrument with similar sample preparation. Size analysis was performed by measuring particle size along the long axis on HAADF-STEM images using the software, ImageJ.

X-ray diffraction. PXRD patterns were collected on a Bruker D2 Phaser powder X-ray diffractometer operated at full power with Cu Ka radiation wavelength (1.54 Å). Data were collected in reflection mode in the 2θ range of $15–65^0$ using a step size of 0.04^0 with scans running for 2 h. Samples were prepared by drop-casting NPL from solution into a thick film on a zero-background offcut Si substrate.

X-ray photoelectron spectroscopy. Samples were prepared by drop-casting NPL from solution into films on a zero-background offcut Si substrate. XPS analysis was performed on a Kratos Axis Nova spectrometer using monochromatic Al Kα source (1486.6 eV). *Cd 3d, Se 3d, O 1s, Cu 2p*, high-resolution spectra were collected using an analysis area of 0.3 x 0.7 mm2 and 20 eV pass energy with the step size of 100 meV. Charge neutralization was performed using a co-axial, low energy (≈ 0.1 eV) electron flood source to avoid shifts in the recovered binding energy. Peak deconvolutions were done with Casa software, version 2.3.24PR1.0. Data were calibrated to adventitious C1s peak set at 284.8 eV. Background intensities are accounted for by applying Shirley background. Line shapes defined by LA(1.53, 243) are numerically integrated Voigt functions. To reproduce data spectrum, these were deconvoluted using 3 doublet peaks indicative of surface oxidation of selenide to selenium or higher.

Small Angle X-ray Scattering. SAXS measurements were performed at Beamline 12-ID-B at the Advanced Photon Source. The X-ray beam (14 keV) was exposed to colloidal samples in capillary tubes and data was collected from 0.03 to 0.8 $Å^{-1}$. The scattering data were collected with a Pilatus 2M detector located about 2 m away from the samples.

ASSOCIATED CONTENT

Supporting Information (file type PDF) contains Figures S1-S7: NPL size distribution after Cu(I) CER, EDS maps at different reaction stages with both Cu(I) and Cu(II), XRD patterns from Cu(II) CER, absorbance, XRD and TEM data from Cu(I, II) chloride reactions. Tables S1 and S2: Summary of EDS and XPS results at different reaction stages with both Cu(I) and Cu(II) CER on 5 ML NPLs.

AUTHOR INFORMATION

Corresponding Author

* Correspondence to: Progna Banerjee ORCID ID: 0000-0003-3257-7317

Author Contributions

P.B. conceptualized the project, performed synthesis and nanomaterial characterizations using XRD, UV-Vis, PLE, HRTEM, EDS, data analyses for HRTEM, XRD, XPS, optical studies, SAXS and wrote the manuscript. A.S. F. conducted the XPS studies. X. Z. helped with the SAXS measurements at APS beamline. B.T.D. helped with synthesis and data analysis. E.V.S. provided project guidance and helped with analysis. All authors have given approval to the final version of the manuscript.

Funding Sources

Work performed at the Center for Nanoscale Materials and Advanced Photon Source, U.S. Department of Energy Office of Science User Facilities, were supported by the U.S. DOE, Office of Basic Energy Sciences, under Contract No. DE-AC02-06CH11357.

ABBREVIATIONS

nanoplatelet, NPL; cadmium selenide, CdSe; cation exchange reaction, CER; energy dispersive spectroscopy, EDS; x-ray diffraction, XRD; x-ray photoelectron spectroscopy, XPS; dark-field transmission electron microscopy, DFTEM.

REFERENCES

(1) Son, D. H.; Hughes, S. M.; Yin, Y.; Paul Alivisatos, A. Cation exchange reactions in ionic nanocrystals. *Science* **2004**, *306* (5698), 1009-1012. DOI: 10.1126/science.1103755

(2) Li, X.; Ji, M.; Li, H.; Wang, H.; Xu, M.; Rong, H.; Wei, J.; Liu, J.; Liu, J.; Chen, W.; et al. Cation/Anion Exchange Reactions toward the Syntheses of Upgraded Nanostructures: Principles and Applications. *Matter* **2020**, *2* (3), 554-586. DOI: 10.1016/j.matt.2019.12.024

(3) Beberwyck, B. J.; Surendranath, Y.; Alivisatos, A. P. Cation Exchange: A Versatile Tool for Nanomaterials Synthesis. *J. Phys. Chem. C* **2013**, *117* (39), 19759-19770. DOI: 10.1021/jp405989z

(4) De Trizio, L.; Manna, L. Forging Colloidal Nanostructures via Cation Exchange Reactions. *Chemical Reviews* **2016**, *116* (18), 10852-10887. DOI: 10.1021/acs.chemrev.5b00739.

(5) Li, H.; Zanella, M.; Genovese, A.; Povia, M.; Falqui, A.; Giannini, C.; Manna, L. Sequential Cation Exchange in Nanocrystals: Preservation of Crystal Phase and Formation of Metastable Phases. *Nano Letters* **2011**, *11* (11), 4964-4970. DOI: 10.1021/nl202927a.

(6) White, S. L.; Banerjee, P.; Jain, P. K. Liquid-like cationic sub-lattice in copper selenide clusters. *Nat Commun* **2017**, *8*, 14514. DOI: 10.1038/ncomms14514

(7) Liang, S.; Liu, X. L.; Yang, Y. Z.; Wang, Y. L.; Wang, J. H.; Yang, Z. J.; Wang, L. B.; Jia, S. F.; Yu, X. F.; Zhou, L.; et al. Symmetric and asymmetric Au-AgCdSe hybrid nanorods. *Nano Lett* **2012**, *12* (10), 5281-5286. DOI: 10.1021/nl3025505

(8) Nelson, H. D.; Hinterding, S. O. M.; Fainblat, R.; Creutz, S. E.; Li, X.; Gamelin, D. R. Mid-Gap States and Normal vs Inverted Bonding in Luminescent Cu+- and Ag+-Doped CdSe Nanocrystals. *J. Am. Chem. Soc.* **2017**, *139* (18), 6411-6421. DOI: 10.1021/jacs.7b01924

(9) Neumann, T.; Feldmann, S.; Moser, P.; Delhomme, A.; Zerhoch, J.; van de Goor, T.; Wang, S.; Dyksik, M.; Winkler, T.; Finley, J. J.; et al. Manganese doping for enhanced magnetic brightening and circular

polarization control of dark excitons in paramagnetic layered hybrid metal-halide perovskites. *Nat Commun* **2021**, *12* (1), 3489. DOI: 10.1038/s41467-021-23602-1

(10) Paul, S.; Bladt, E.; Richter, A. F.; Döblinger, M.; Tong, Y.; Huang, H.; Dey, A.; Bals, S.; Debnath, T.; Polavarapu, L.; et al. Manganese-Doping-Induced Quantum Confinement within Host Perovskite Nanocrystals through Ruddlesden–Popper Defects. *Angew Chem Int Ed Engl* **2020**, *59* (17), 6794-6799. DOI: 10.1002/anie.201914473

(11) Hodges, J. M.; Kletetschka, K.; Fenton, J. L.; Read, C. G.; Schaak, R. E. Sequential Anion and Cation Exchange Reactions for Complete Material Transformations of Nanoparticles with Morphological Retention. *Angewandte Chemie International Edition* **2015**, *54* (30), 8669-8672. DOI: 10.1002/anie.201504099

(12) Rakowska, P. D.; Tiddia, M.; Faruqui, N.; Bankier, C.; Pei, Y.; Pollard, A. J.; Zhang, J.; Gilmore, I. S. Antiviral surfaces and coatings and their mechanisms of action. *Communications Materials* **2021**, *2* (1), 53. DOI: 10.1038/s43246-021-00153-y.

(13) Guan, M.; Zhou, Z.; Mei, L.; Zheng, H.; Ren, W.; Wang, L.; Du, Y.; Jin, D.; Zhou, J. Direct cation exchange of surface ligand capped upconversion nanocrystals to produce strong luminescence. *Chem. Commun.* **2018**, *54* (69), 9587-9590. DOI: 10.1039/C8CC04924F

(14) Licht, S. Aqueous Solubilities, Solubility Products and Standard Oxidation-Reduction Potentials of the Metal Sulfides. *J. Electrochem. Soc.* **1988**, *135* (12), 2971. DOI: 10.1149/1.2095471

(15) Jharimune, S.; Sathe, A. A.; Rioux, R. M. Solvent-Dependent Impact of Spectator Anions on the Thermodynamics of Cation Exchange in CdSe Nanocrystals. *J. Phys. Chem. C* **2021**, *125* (23), 12792-12801. DOI: 10.1021/acs.jpcc.1c03031

(16) Ott, F. D.; Spiegel, L. L.; Norris, D. J.; Erwin, S. C. Microscopic Theory of Cation Exchange in CdSe Nanocrystals. *Physical Review Letters* **2014**, *113* (15), 156803. DOI: 10.1103/PhysRevLett.113.156803.

(17) Shannon, R. D. Revised Effective Ionic Radii and Systematic Studies of Interatomic Distances in Halides and Chalcogenides. In *Acta Cryst*, 1976.

(18) Lee, S.; Yoon, D.-E.; Kim, D.; Shin, D. J.; Jeong, B. G.; Lee, D.; Lim, J.; Bae, W. K.; Lim, H.-K.; Lee, D. C. Direct cation exchange of CdSe nanocrystals into ZnSe enabled by controlled binding between guest cations and organic ligands. *Nanoscale* **2019**, *11* (32), 15072-15082, 10.1039/C9NR05195C. DOI: 10.1039/C9NR05195C.

(19) Dufour, M.; Izquierdo, E.; Livache, C.; Martinez, B.; Silly, M. G.; Pons, T.; Lhuillier, E.; Delerue, C.; Ithurria, S. Doping as a Strategy to Tune Color of 2D Colloidal Nanoplatelets. *ACS Applied Materials & Interfaces* **2019**, *11* (10), 10128-10134. DOI: 10.1021/acsami.8b18650.

(20) Bouet, C.; Laufer, D.; Mahler, B.; Nadal, B.; Heuclin, H.; Pedetti, S.; Patriarche, G.; Dubertret, B. Synthesis of Zinc and Lead Chalcogenide Core and Core/Shell Nanoplatelets Using Sequential Cation Exchange Reactions. *Chem. Mater.* **2014**, *26* (9), 3002-3008. DOI: 10.1021/cm5008608

(21) Dabard, C.; Planelles, J.; Po, H.; Izquierdo, E.; Makke, L.; Gréboval, C.; Moghaddam, N.; Khalili, A.; Dang, T. H.; Chu, A.; et al. Optimized Cation Exchange for Mercury Chalcogenide 2D Nanoplatelets and Its Application for Alloys. *Chem. Mater.* **2021**, *33* (23), 9252-9261. DOI: 10.1021/acs.chemmater.1c02951

(22) De Trizio, L.; Li, H.; Casu, A.; Genovese, A.; Sathya, A.; Messina, G. C.; Manna, L. Sn Cation Valency Dependence in Cation Exchange Reactions Involving Cu2-xSe Nanocrystals. *Journal of the American Chemical Society* **2014**, *136* (46), 16277-16284. DOI: 10.1021/ja508161c.

(23) Xu, W.; Liu, H.; Zhou, D.; Chen, X.; Ding, N.; Song, H.; Ågren, H. Localized surface plasmon resonances in self-doped copper chalcogenide binary nanocrystals and their emerging applications. *Nano Today* **2020**, *33*, 100892. DOI: 10.1016/j.nantod.2020.100892

(24) Mitzi, D. B.; Kim, Y. Spiers Memorial Lecture: Next generation chalcogenide-based absorbers for thin-film solar cells. *Faraday Discuss.* **2022**, *239* (0), 9-37. DOI: 10.1039/D2FD00132B

(25) Wu, L.; Wang, Q.; Zhuang, T.-T.; Zhang, G.-Z.; Li, Y.; Li, H.-H.; Fan, F.-J.; Yu, S.-H. A library of polytypic copper-based quaternary sulfide nanocrystals enables efficient solar-to-hydrogen conversion. *Nat Commun* **2022**, *13* (1), 5414. DOI: 10.1038/s41467-022-33065-7
(26) Zhao, Y.; Burda, C. Development of plasmonic semiconductor nanomaterials with copper chalcogenides for a future with sustainable energy materials. *Energy Environ. Sci.* **2012**, *5* (2), 5564-5576. DOI: 10.1039/c1ee02734d.
(27) Zhang, Y.; Xing, C.; Liu, Y.; Spadaro, M. C.; Wang, X.; Li, M.; Xiao, K.; Zhang, T.; Guardia, P.; Lim, K. H.; et al. Doping-mediated stabilization of copper vacancies to promote thermoelectric properties of Cu2−xS. *Nano Energy* **2021**, *85*, 105991. DOI: 10.1016/j.nanoen.2021.105991
(28) Kush, P.; Deka, S. Multifunctional Copper-Based Quaternary Chalcogenide Semiconductors Toward State-of-the-Art Energy Applications. *ChemNanoMat* **2019**, *5* (4), 373-402. DOI: 10.1002/cnma.201800321
(29) Lesnyak, V.; Brescia, R.; Messina, G. C.; Manna, L. Cu Vacancies Boost Cation Exchange Reactions in Copper Selenide Nanocrystals. *J Am Chem Soc* **2015**, *137* (29), 9315-9323. DOI: 10.1021/jacs.5b03868
(30) Pruthvija, B.; Lakshmi, K. P.; Nagashree, K. L. Copper chalcogenides for rechargeable batteries. *Materials Today: Proceedings* **2022**, *65*, 3253-3258. DOI: 10.1016/j.matpr.2022.05.381
(31) Heyding, R. D.; Murray, R. M. The crystal structures of Cu1•8Se, Cu3Se2, α- and γCuSe, CuSe2, and CuSe2II. *Can. J. Chem.* **1976**, *54* (6), 841-848. DOI: 10.1139/v76-122
(32) Xie, Y.; Zheng, X.; Jiang, X.; Lu, J.; Zhu, L. Sonochemical synthesis and mechanistic study of copper selenides Cu(2-x)Se, beta-CuSe, and Cu(3)Se(2). *Inorganic Chemistry* **2002**, *41* (2), 387-392. DOI: 10.1021/ic010108v
(33) White, S. L.; Banerjee, P.; Chakraborty, I.; Jain, P. K. Ion Exchange Transformation of Magic-Sized Clusters. *Chem. Mater.* **2016**, *28* (22), 8391-8398. DOI: 10.1021/acs.chemmater.6b03882
(34) Xue, M.-Z.; Zhou, Y.-N.; Zhang, B.; Yu, L.; Zhang, H.; Fu, Z.-W. Fabrication and Electrochemical Characterization of Copper Selenide Thin Films by Pulsed Laser Deposition. *J. Electrochem. Soc.* **2006**, *153* (12), A2262. DOI: 10.1149/1.2358854
(35) Gosavi, S. R.; Deshpande, N. G.; Gudage, Y. G.; Sharma, R. Physical, optical and electrical properties of copper selenide (CuSe) thin films deposited by solution growth technique at room temperature. *Journal of Alloys and Compounds* **2008**, *448* (1), 344-348. DOI: 10.1016/j.jallcom.2007.03.068
(36) Takano, Y.; Uchiyama, N.; Ogawa, S.; Môri, N.; Kimishima, Y.; Arisawa, S.; Ishii, A.; Hatano, T.; Togano, K. Superconducting properties of CuS2−xSex under high pressure. *Physica C: Superconductivity* **2000**, *341-348*, 739-740. DOI: 10.1016/S0921-4534(00)00669-9
(37) Krill, G.; Panissod, P.; Lapierre, M. F.; Gautier, F.; Robert, C.; Eddine, M. N. Magnetic properties and phase transitions of the metallic CuX2 dichalcogenides (X=S, Se, Te) with pyrite structure. *J. Phys. C: Solid State Phys.* **1976**, *9* (8), 1521. DOI: 10.1088/0022-3719/9/8/023
(38) Banerjee, P.; Jain, P. K. Lithiation of Copper Selenide Nanocrystals. *Angew Chem Int Ed Engl* **2018**, *57* (30), 9315-9319. DOI: 10.1002/anie.201803358
(39) Yang, L.; Knowles, K. E.; Gopalan, A.; Hughes, K. E.; James, M. C.; Gamelin, D. R. One-Pot Synthesis of Monodisperse Colloidal Copper-Doped CdSe Nanocrystals Mediated by Ligand–Copper Interactions. *Chem. Mater.* **2016**, *28* (20), 7375-7384. DOI: 10.1021/acs.chemmater.6b02869
(40) Singh, S.; Tomar, R.; ten Brinck, S.; De Roo, J.; Geiregat, P.; Martins, J. C.; Infante, I.; Hens, Z. Colloidal CdSe Nanoplatelets, A Model for Surface Chemistry/Optoelectronic Property Relations in Semiconductor Nanocrystals. *J. Am. Chem. Soc.* **2018**, *140* (41), 13292-13300. DOI: 10.1021/jacs.8b07566
(41) Wang, Y.; Zhukovskyi, M.; Tongying, P.; Tian, Y.; Kuno, M. Synthesis of Ultrathin and Thickness-Controlled Cu2-xSe Nanosheets via Cation Exchange. *J Phys Chem Lett* **2014**, *5* (21), 3608-3613. DOI: 10.1021/jz5019288
(42) Sharma, M.; Olutas, M.; Yeltik, A.; Kelestemur, Y.; Sharma, A.; Delikanli, S.; Guzelturk, B.; Gungor, K.; McBride, J. R.; Demir, H. V. Understanding the Journey of Dopant Copper Ions in Atomically Flat Colloidal

Nanocrystals of CdSe Nanoplatelets Using Partial Cation Exchange Reactions. *Chem. Mater.* **2018**, *30* (10), 3265-3275. DOI: 10.1021/acs.chemmater.8b00196
(43) Sharma, M.; Gungor, K.; Yeltik, A.; Olutas, M.; Guzelturk, B.; Kelestemur, Y.; Erdem, T.; Delikanli, S.; McBride, J. R.; Demir, H. V. Near-Unity Emitting Copper-Doped Colloidal Semiconductor Quantum Wells for Luminescent Solar Concentrators. *Advanced Materials* **2017**, *29* (30), 1700821. DOI: 10.1002/adma.201700821
(44) Ithurria, S.; Talapin, D. V. Colloidal atomic layer deposition (c-ALD) using self-limiting reactions at nanocrystal surface coupled to phase transfer between polar and nonpolar media. *J Am Chem Soc* **2012**, *134* (45), 18585-18590. DOI: 10.1021/ja308088d
(45) Ithurria, S.; Tessier, M. D.; Mahler, B.; Lobo, R. P. S. M.; Dubertret, B.; Efros, A. L. Colloidal nanoplatelets with two-dimensional electronic structure. *Nature Materials* **2011**, *10* (12), 936-941. DOI: 10.1038/nmat3145
(46) Zhu, C.; Chen, D.; Cao, W.; Lai, R.; Pu, C.; Li, J.; Kong, X.; Peng, X. Facet-Dependent On-Surface Reactions in the Growth of CdSe Nanoplatelets. *Angewandte Chemie International Edition* **2019**, *58* (49), 17764-17770. DOI: 10.1002/anie.201909576
(47) Yeltik, A.; Delikanli, S.; Olutas, M.; Kelestemur, Y.; Guzelturk, B.; Demir, H. V. Experimental Determination of the Absorption Cross-Section and Molar Extinction Coefficient of Colloidal CdSe Nanoplatelets. *J. Phys. Chem. C* **2015**, *119* (47), 26768-26775. DOI: 10.1021/acs.jpcc.5b09275
(48) White, S. L.; Smith, J. G.; Behl, M.; Jain, P. K. Co-operativity in a nanocrystalline solid-state transition. *Nat Commun* **2013**, *4*, 2933. DOI: 10.1038/ncomms3933
(49) Khammang, A.; Wright, J. T.; Meulenberg, R. W. Mechanistic insight into copper cation exchange in cadmium selenide semiconductor nanocrystals using X-ray absorption spectroscopy. *Nat Commun* **2021**, *12* (1), 438. DOI: 10.1038/s41467-020-20712-0
(50) White, S. L.; Smith, J. G.; Behl, M.; Jain, P. K. Co-operativity in a nanocrystalline solid-state transition. *Nat Commun* **2013**, *4* (1), 2933. DOI: 10.1038/ncomms3933
(51) White, S. L.; Banerjee, P.; Jain, P. K. Liquid-like cationic sub-lattice in copper selenide clusters. *Nat Commun* **2017**, *8* (1), 14514. DOI: 10.1038/ncomms14514
(52) Jana Santanu , D. P., Abécassis Benjamin CdSe Nanoplatelets: Living Polymers. *Angewandte Chemie International Edition Communication* **2016**, *55* (32), 9371-9374. DOI: https://doi.org/10.1002/anie.201603880.
(53) Guillemeney, L.; Lermusiaux, L.; Landaburu, G.; Wagnon, B.; Abecassis, B. Curvature and self-assembly of semi-conducting nanoplatelets. *Commun Chem* **2022**, *5* (1), 7. DOI: 10.1038/s42004-021-00621-z
(54) Nicolo Castro, C. B., Sandrine Ithurria, Nicolas Lequeux, Doru Constantin, Pierre Levitz, Diego Pontoni, and Benjamin Abécassis. Insights into the Formation Mechanism of CdSe Nanoplatelets Using in Situ X-ray Scattering. *Nano Letters* **2019**, *19* (9), 6466-6474. DOI: 10.1021/acs.nanolett.9b02687.
(55) Singh, S.; Tomar, R.; Ten Brinck, S.; De Roo, J.; Geiregat, P.; Martins, J. C.; Infante, I.; Hens, Z. Colloidal CdSe Nanoplatelets, A Model for Surface Chemistry/Optoelectronic Property Relations in Semiconductor Nanocrystals. *J Am Chem Soc* **2018**, *140* (41), 13292-13300. DOI: 10.1021/jacs.8b07566
(56) Parr, R. G.; Pearson, R. G. Absolute hardness: companion parameter to absolute electronegativity. *J. Am. Chem. Soc.* **1983**, *105* (26), 7512-7516. DOI: 10.1021/ja00364a005
(57) Pearson, R. G. Chemical hardness and density functional theory. *J Chem Sci* **2005**, *117* (5), 369-377. DOI: 10.1007/BF02708340
(58) Pearson, R. G. Absolute electronegativity and hardness: application to inorganic chemistry. *Inorganic Chemistry* **1988**, *27* (4), 734-740. DOI: 10.1021/ic00277a030
(59) Fagan, A. M.; Steimle, B. C.; Schaak, R. E. Orthogonal reactivity and interface-driven selectivity during cation exchange of heterostructured metal sulfide nanorods. *Chem. Commun.*, **2022**, 58, 4328-4331.DOI: 10.1039/D1CC07190D.

(60) Laoire, C. O.; Mukerjee, S.; Abraham, K. M.; Plichta, E. J.; Hendrickson, M. A. Influence of Nonaqueous Solvents on the Electrochemistry of Oxygen in the Rechargeable Lithium−Air Battery. *J. Phys. Chem. C* **2010**, *114* (19), 9178-9186. DOI: 10.1021/jp102019y.
(61) Grillo, I. B.; Einloft, S.; Seferin, M. Assessing Thermodynamic Data of CO2 capture by Ionic Liquids through Hard and Soft Base THeory. *Energy Procedia* **2017**, *114*, 81-85. DOI: 10.1016/j.egypro.2017.03.1150
(62) Coropceanu, I.; Janke, E. M.; Portner, J.; Haubold, D.; Nguyen, T. D.; Das, A.; Tanner, C. P. N.; Utterback, J. K.; Teitelbaum, S. W.; Hudson, M. H.; et al. Self-assembly of nanocrystals into strongly electronically coupled all-inorganic supercrystals. *Science* **2022**, *375* (6587), 1422-1426. DOI: 10.1126/science.abm6753
(63) Mondal, P.; Sinha, A.; Salam, N.; Roy, A. S.; Jana, N. R.; Islam, S. M. Enhanced catalytic performance by copper nanoparticle–graphene based composite. *RSC Adv.* **2013**, *3* (16), 5615-5623. DOI: 10.1039/C3RA23280H
(64) Li, Z.; Zhai, L.; Ma, T.; Zhang, J.; Wang, Z. Efficient and Stable Catalytic Hydrogen Evolution of ZrO2/CdSe-DETA Nanocomposites under Visible Light. *Catalysts* **2022**, *12* (11), 1385. DOI: 10.3390/catal12111385
(65) McCormick, C. R.; Schaak, R. E. Simultaneous Multication Exchange Pathway to High-Entropy Metal Sulfide Nanoparticles. *Journal of the American Chemical Society* **2021**, *143* (2), 1017-1023. DOI: 10.1021/jacs.0c11384.
(66) Tao, H.; Wu, T.; Aldeghi, M.; Wu, T. C.; Aspuru-Guzik, A.; Kumacheva, E. Nanoparticle synthesis assisted by machine learning. *Nature Reviews Materials* **2021**, *6* (8), 701-716. DOI: 10.1038/s41578-021-00337-5.

TOC Graphic